ChemCatChem

Research Article
doi.org/10.1002/cctc.202301228

Chemistry Europe
European Chemical Societies Publishing

www.chemcatchem.org

Pushing the Efficiency of the Selective and Base-Free Air-Oxidation of HMF by Varying the Properties of Carbon-Based Supports

Dominik Neukum,[a] Erisa Saraçi,[a, b] Bärbel Krause,[c] Ajai Raj Lakshmi Nilayam,[d, e] Alisa Sinigalia,[c] and Jan-Dierk Grunwaldt*[a, b]

The selective oxidation of 5-(Hydroxymethyl)furfural (HMF) to 2,5-Furandicarboxylic acid (FDCA) is highly attractive for the production of renewable monomers as substitute for fossil-based monomers. To achieve a sustainable synthesis, we report on advances for a base-free approach, reducing waste from the process, using air as oxidant and heterogeneous catalysts. Various Carbon-based supports, which can be bio-sourced and cost-efficient, for Pt particles were investigated as they allow for an easy reuse and at the end-of-life Pt can be recycled to enable a closed cycle. Commercially available supports with varying properties, which might replace the base, were studied with Pt particles of similar size and loading. Significant differences in the catalytic activity were observed, which were correlated with the O-functionalities and graphitization degree of the supports derived from Raman spectroscopy, temperature-programmed desorption, and X-ray photoelectron spectroscopy. An activated carbon (Norit ROX) rich in quinone/pyrone-type groups and a carbon black-based catalyst with graphene-layers pushed the efficiency with enhanced FDCA-yields enabling the complete substitution of the homogeneous base. This allows to circumvent the base in this process which together with high selectivity, air as oxidant, a reusable catalyst, and the use of bio-based feedstock contributes to the sustainability of the production of renewable monomers.

Introduction

In recent years, the use of biomass as a renewable feedstock for chemical products has attracted huge interest.[1] This shift of feedstock reduces the consumption of fossil resources, and a short carbon cycle is achieved. The approach is particularly interesting for chemicals with low H/C-ratio e.g. containing oxygen functionalities.[2] One promising example of renewable substitute chemicals is the use of 5-(Hydroxymethyl)furfural (HMF) for the production, e.g., of aromatic carboxylic acids like 2,5-Furandicarboxylic acid (FDCA).[3] The synthesis of HMF can be performed using different bio-based feedstock, such as cellulose or inulin from by-products of the agricultural industry.[4] HMF can be easier transformed into value-added products, e.g., *via* selective oxidation, than fossil-derived compounds like hexane or benzene. There are multiple methods for the oxidation of HMF including stoichiometric reagents, electrochemical catalysis, homogeneous catalysis, bio catalysis and heterogeneous thermal catalysis.[1b] Due to the easy separation of the catalyst, the use of heterogeneous catalysis is advantageous.

For this, solid catalysts based on noble metals (Au, Pt, Pd, Ru) are often reported in literature.[1b] The base-free oxidation of HMF usually proceeds via the intermediates 2,5-Diformylfuran (DFF) and 5-Formyl-2-furancarboxylic acid (FFCA; scheme 1).[5] To increase the solubility of FDCA in water during oxidation, often a homogeneous base is added to the solution. This leads also to an enhancement of the reaction rate.[6] However, many groups strive to achieve a successful FDCA synthesis under base-free conditions that would avoid additional waste in the product separation, and thus attain a greener process.[7]

In this work, we focus on the use of carbon-based support materials to produce FDCA using a heterogeneous catalyst under base-free conditions with air as oxidant. These carbon supports can be derived from renewable C-sources and are low cost materials.[8] In addition, they allow not only the re-use of the catalyst but also easier recyclability of the noble metal as

[a] D. Neukum, Dr. E. Saraçi, Prof. Dr. J.-D. Grunwaldt
Institute of Catalysis Research and Technology
Karlsruhe Institute of Technology
Hermann-von-Helmholtz-Platz 1, 76344 Eggenstein-Leopoldshafen
E-mail: grunwaldt@kit.edu

[b] Dr. E. Saraçi, Prof. Dr. J.-D. Grunwaldt
Institute for Chemical Technology and Polymer Chemistry
Karlsruhe Institute of Technology
Engesserstraße 20, 76131 Karlsruhe

[c] Dr. B. Krause, A. Sinigalia
Institute for Photon Science and Synchrotron Radiation
Karlsruhe Institute of Technology
Hermann-von-Helmholtz-Platz 1, 76344 Eggenstein-Leopoldshafen

[d] A. R. Lakshmi Nilayam
Institute of Nanotechnology
Karlsruhe Institute of Technology
Hermann-von-Helmholtz-Platz 1, 76344 Eggenstein-Leopoldshafen

[e] A. R. Lakshmi Nilayam
Karlsruhe Nano Micro Facility (KNMFi)
Karlsruhe Institute of Technology
Hermann-von-Helmholtz-Platz 1, 76344 Eggenstein-Leopoldshafen

Supporting information for this article is available on the WWW under https://doi.org/10.1002/cctc.202301228

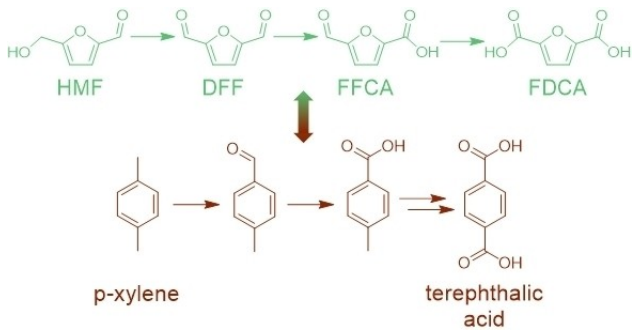

Scheme 1. Reaction scheme for HMF oxidation to FDCA compared to the classical oxidation of p-xylene to terephthalic acid.

the support can be burnt. Artz et al. reported the base-free oxidation of HMF, employing Ru supported by a covalent triazine framework with a FDCA yield of 41.4% after 1 h.[9] Pt supported on activated carbon was shown to oxidize HMF to FDCA under base-free conditions.[10] However, only low FDCA yields were obtained due to slow hydration of the aldehyde function. Yu et al. achieved a FDCA yield of >99% with Pt supported on activated carbon obtained from carbonizing chitosan.[11] The authors concluded that the adsorption of Pt, and hence the catalyst activity, improved with a lower O-content of the support. The influence of basicity of N-doped carbons as support for Pt-based catalysts was investigated by Han et al.[12] A maximum FDCA yield of 96% after 12 h (110 °C) was obtained with a C-support containing a high amount of pyridine-type N. Zhou et al. observed a superior activity of Pt supported on carbon nanotubes (CNT) with a FDCA-selectivity of 98% after 14 h (95 °C).[13] Furthermore, they functionalized the CNTs and analyzed the concentration of O-containing functional groups by temperature-programmed desorption (TPD) in Ar. The authors found that either carbonyl/quinone or phenol groups lead to an increase in the activity of the catalysts. While the findings of Zhou et al. underscore the significant influence of O-containing functional groups, their insights are confined to well-defined carbon nanotube materials.[13] For better transferability to industrial settings, comprehensive property-activity relationships, concerning both O-functionalities and graphitization degree, must be explored for heterogeneous applied materials, such as activated carbons. These materials can be easily processed into thicker shapes, facilitating scale-up and catalyst separation in industrial processes.[14] In addition, catalysts supported on activated carbon exhibit high catalytic activity compared to other carbon-based supports.[15]

In this work, we present the oxidation of HMF with air using Pt-based catalysts supported on different activated carbon (denoted as: ROX, CN1, DARCO) and carbon black (denoted as: Vulcan, CBA) materials. The supports were comprehensively characterized by TPD of CO and CO_2, X-ray photoelectron spectroscopy (XPS), Raman spectroscopy, elemental analysis, and nitrogen physisorption to identify the role of their chemical properties. In addition, we used X-ray absorption spectroscopy (XAS) and scanning transmission electron microscopy (STEM) for characterization of the Pt particles, to ensure a comparable loading and particle size for this systematic study. Depending on the support properties, a replacement of the homogeneous base by the support material could be achieved while ensuring a high selectivity to FDCA. In this way, a knowledge-based approach for the selection of the carbon support for a more sustainable, base-free air-oxidation of HMF to the bio-based monomer FDCA is opened up.

Results and Discussion

Characterization of Pt Particles

First, the Pt particles were characterized to ensure a similar Pt loading, particle size and reduction degree. This allows us to systematically study the influence of the support properties on the catalytic activity by eliminating the variable of the active Pt-phase. The Pt loading of all catalysts was comparable in the range of 1.6 to 2 wt.%, as determined by inductively coupled plasma optical emission spectrometry (ICP-OES; Table 1). The degree of the catalyst reduction was estimated from X-ray absorption near edge structure (XANES) spectra at Pt L_3-edge. We found only slight differences in the degree of reduction which lied in between 70 and 89% metallic Pt (Figure 1 and Figure S12–S17).

The mean Pt particle diameter of the catalysts was determined by STEM analysis to be in the range of 1.1 (Pt/CN1) to 1.7 nm (Pt/DARCO and Pt/CBA), with a narrow size distribution (Figure 2; cf. Figure S1–S7). The small particle diameter

Table 1. Pt loading of the catalysts as determined by ICP-OES. The support material used for the synthesis is specified in the right column.

Catalyst	Pt loading/wt.%	Support material
Pt/ROX	1.7±0.1	NORIT® Type ROX 0.8
Pt/CN1	2.0±0.1	NORIT® CN1®
Pt/DARCO	1.6±0.1	NORIT® DARCO®
Pt/Vulcan	1.7±0	Carbon black Vulcan® XC72
Pt/CBA	1.7±0.2	Carbon black acetylene (Alfa Aesar)

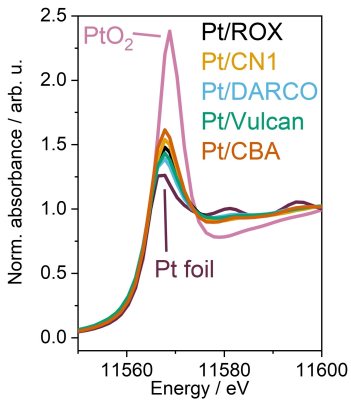

Figure 1. Normalized XANES spectra of the catalysts measured at Pt L_3-edge. PtO_2 and Pt foil reference are shown.

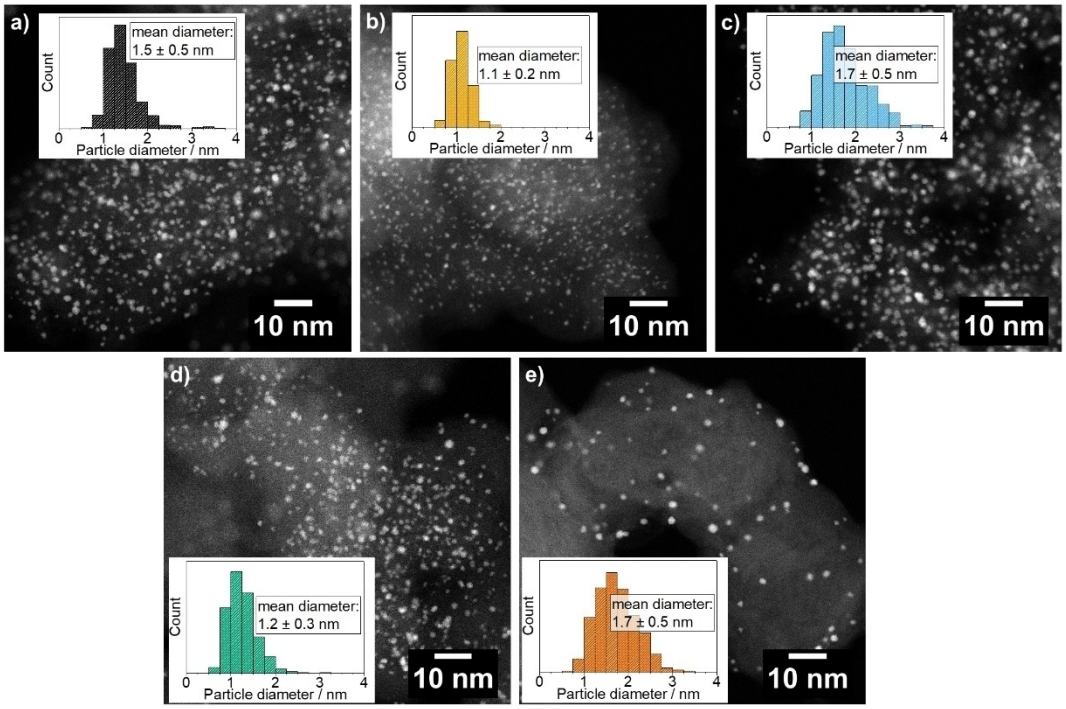

Figure 2. STEM image and particle size distribution (n: total particle count) of a) Pt/ROX (n = 539), b) Pt/CN1 (n = 469), c) Pt/DARCO (n = 670), d) Pt/Vulcan (n = 777), and e) Pt/CBA (n = 451).

allows for an efficient use of Pt in the catalysts due to the high surface-atom fraction. The Pt dispersion varied between 66% for Pt/DARCO and Pt/CBA and close to 100% for Pt/CN1 (Table S2) with an almost linear dependency (Figure S8). The X-ray diffraction (XRD) pattern (cf. Figure S11) showed broad or no reflections of metallic Pt besides the carbon reflections for all catalysts, indicating a small particle size.[16] Pt/DARCO additionally displayed sharp reflections, which might be related to graphite (2θ at 26.6°) from extended graphite lattices in the support. In addition, they might be caused from ash in the activated carbon, but they could not be identified unequivocally.

Catalytic Testing

All catalysts were tested for the aerobic oxidation of HMF under base-free conditions (100 °C, 30 bar synthetic air), with the aim to achieve a good atom economy with FDCA ideally being the only product (Figure 3 (a)). For Pt/CBA, the concentration of DFF and FFCA increased rapidly in the first reaction hours, and the HMF conversion reached >99% after 5 h (Figure 3 (b)). After 2 h the concentration of FFCA decreased steadily while FDCA increased. Similar results were obtained for all catalysts. In contrast to other studies on the base-free oxidation, no formation of 5-(Hydroxymethyl)furan-2-carboxylic acid was observed.[17]

When comparing the FDCA yield for the five different catalysts, we observed considerable differences (Figure 3 (a) and Table S3). Pt/CBA gave the highest FDCA yield with 87% after 7 h reaction time, and Pt/ROX had a FDCA yield of 75%. Both catalysts are highly active compared to other catalysts reported in literature (cf. Table S5). This is particularly interesting, since the use of air leads to lower reaction rates compared to pure oxygen.[5] Interestingly, Pt/DARCO yields only about 50% of the FDCA yield of Pt/CBA. Given the nearly identical particle size distribution and mean particle diameter of Pt/CBA, size-dependent effects on the catalytic activity were minimal, especially when compared to the influence exerted by the support properties. In addition, the FDCA yield was plotted against the Pt dispersion and the specific Pt surface area (Figure S9 and Figure S10). Again, Pt/DARCO gives a similar dispersion and specific Pt surface area as Pt/CBA, but both exhibit huge differences in the FDCA yield. Thus, only a marginal influence of the Pt dispersion on the catalytic activity is observed. If Pt/DARCO is not taken into account, one might speculate an increase of the FDCA yield with decreasing Pt dispersion exists; however, systematic studies are needed in the future to determine a potential influence of the Pt dispersion. First insights were only obtained for Au-based catalysts.[18] In general, the true amount of active sites for the oxidation in liquid phase may differ from the values calculated for the metal dispersion, specifically due to the bulky HMF.

Pt in Pt/CBA had almost the same reduction degree as in Pt/CN1, which in turn gave the lowest FDCA yield. Minor differences in the reduction degree should not influence the catalytic activity. Therefore, a closer look has to be taken on the influence of the support material.[15,19]

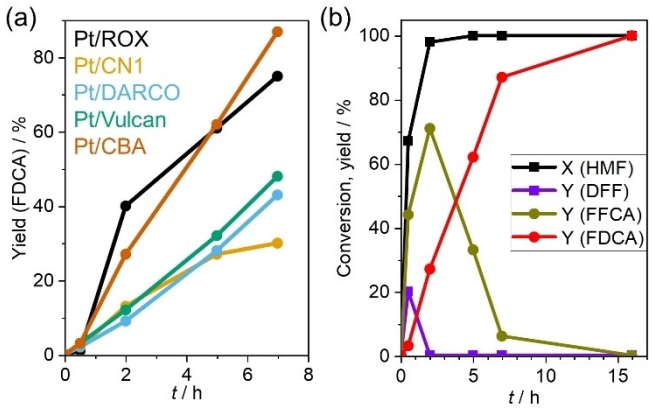

Figure 3. (a) Evolution of the FDCA yield over 7 h reaction time (100 °C, 30 bar synthetic air, HMF:M 100 : 1) for all catalysts (complete catalytic data: Table S3), (b) Conversion of HMF and evolution of the product distribution over 16 h reaction time with Pt/CBA.

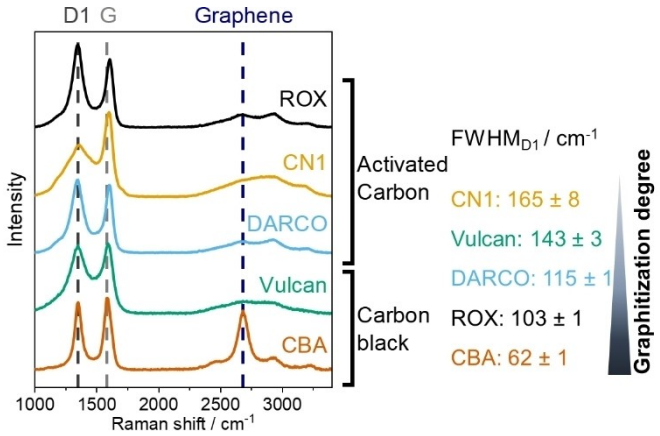

Figure 4. Raman spectra of ROX, CN1, DARCO, Vulcan, and CBA. The positions of D1 and G band are shown in grey, dashed lines and the band associated to graphene in blue dashed line. The FWHM of the D1 band for each support is given on the right side.

Support Characterization

In the following, the activity of the different catalysts is evaluated based on the properties of the support materials, in particular graphite domains for carbon black and O-containing functional groups for activated carbon. Due to huge structural differences of activated carbon and carbon black, they are discussed separately. The O-content of the supports varied from $<1\,\%$ for the two carbon blacks (Vulcan and CBA) to 10.1 % for CN1. However, no systematic variation of the catalytic activity related to the overall O-content was observed. None of the used supports had a significant N-content (≤ 0.4 wt.%), which might contribute to the activity of the catalysts by alkaline sites as shown by Han et al. (cf. Table S6).[12] Furthermore, the specific surface area of the supports (cf. Table S7) did not have an effect on the FDCA yield achieved after 7 h. Thus, the chemical properties of the supports should be responsible for the strong influence on the activity.[20]

All support materials were characterized by Raman spectroscopy to determine the graphitization degree.[15,21] Details on the fitting procedure and assignment of the peaks can be found in the experimental section. Sadezky et al.[22] proposed to use the FWHM of the D1 band to compare the share of graphite domains in carbonaceous materials (Figure 4), with lower FWHM representing higher graphitization degree. CBA support showed by far the highest graphite share. In addition, for CBA a dominant 2D band was visible in the Raman spectrum (Figure 4) at 2680 cm^{-1}, which is the second order overtone of the D band.[23] The sharp peak can be assigned to the presence of one to three layers graphene on the surface of the support.[23] This band typically decreases in intensity and gets broader for extended stacked graphene layers in graphite structures, which is the case for all other samples. We propose that these graphene layers are the origin of the higher activity of Pt/CBA compared to Pt/Vulcan, since both supports have a similar elemental composition. The π-electrons, present in graphene, might promote the dissociative adsorption of O_2.[24] Moreover, it was shown that π-electrons in graphene domains contribute to the Lewis basicity of carbons with low N- and O-content due to resonance stabilization of a charge in the conjugated system and interaction of protons with delocalized π-electrons.[24–25] This could improve the activation, e.g., of alcohol groups, leading to an improved activity of the catalyst.[26]

As Cuesta et al. pointed out, the influence of disordering and band widening due to defects on the shape and intensity of the D1 band leads to uncertainties, which is particularly expected for Vulcan where a considerable overlapping with D3 and D4 peaks was found (Figure S23–S27).[27] Interestingly, ROX and DARCO have a similar graphite share according to FWHM of the D1 band. Despite of this, both catalysts differed by $>30\,\%$ in the FDCA yield after 7 h (Table S3), implying that the different catalytic activity for activated carbon materials could be related to the O-containing functional groups. Raman spectra of the fresh catalysts revealed only slight variations in intensity, with no noticeable differences in the peak shape (Figure S28–S29).

The type and fraction of different O-containing functional groups on the surface of particularly activated carbons, was examined by TPD and XPS. The TPD experiments were first performed with the Pt-based catalysts and afterwards compared to the raw support materials, which gave an improved signal (Figure 5). Since no oxygen was found in elemental analysis (Table S6), neither CBA nor Vulcan displayed any noticeable signal of CO_2 or CO release during TPD (Figure 5 c) + d)). Note that Pt might catalyze secondary reactions. Thus, the differences in the activity of carbon black supports should be ascribed to the carbon structure as assessed by Raman spectroscopy. The assignment of the peaks was based on the literature and analysis of model compounds was not within the scope of this work. For the CO signal, we assigned the peaks to anhydride, alcohol, ether, carbonyl, quinone, and pyrone-type species.[21,28] In case of CO_2, carboxylic acid, anhydride, and lactone species were taken into account.[28] Due to the variation of desorption temperatures for different lactone/ester species, we used two peaks for fitting these species.[28a] More details can

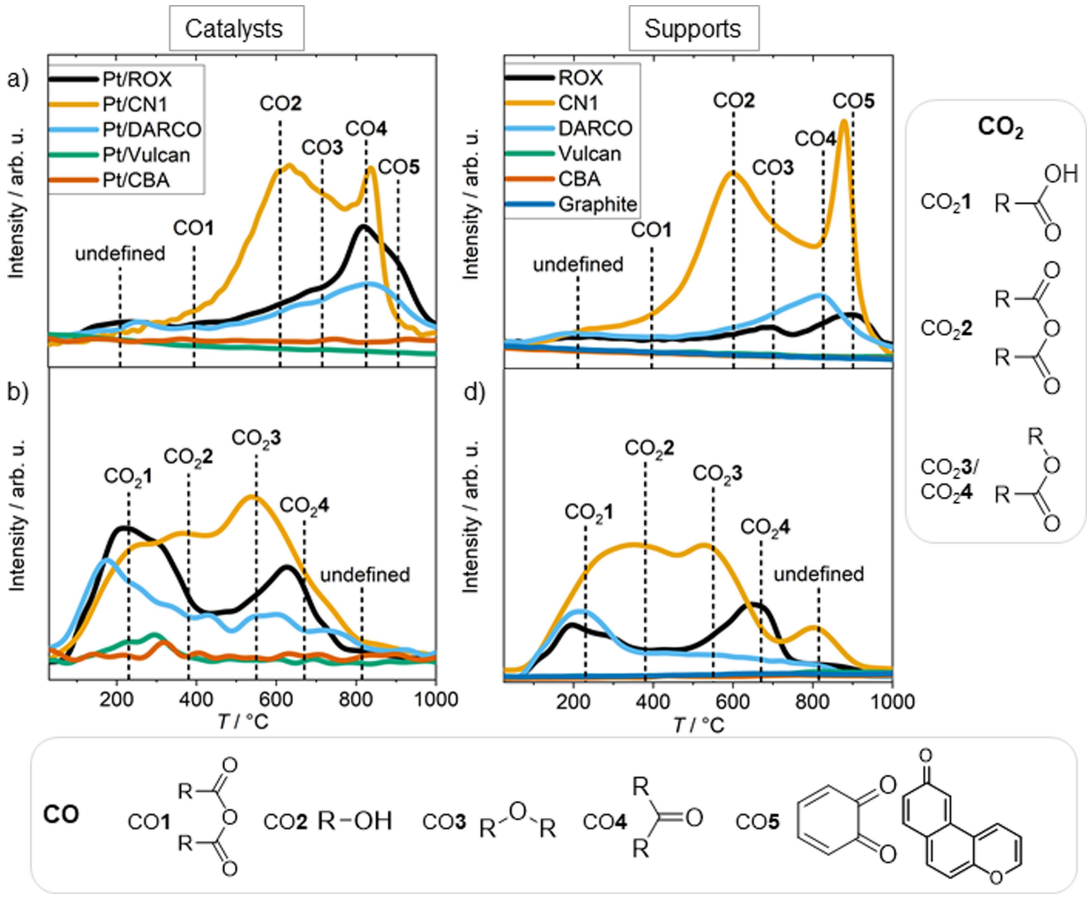

Figure 5. TPD of a) + b) Pt/ROX, Pt/CN1, Pt/DARCO, Pt/Vulcan, Pt/CBA, and c) + d) ROX, CN1, DARCO, Vulcan, CBA. a) + c) show the signal for CO release and b) + d) show the signal for CO_2 release (heating rate: 5 °C min^{-1}, Ar flow: 80 mL min^{-1}).

be found in the experimental section and the supporting information.

For the catalysts based on activated carbon supports (Pt/ROX, Pt/CN1, Pt/DARCO), we observed a small CO release (Figure 5 (a), Figure S30-S32 and Table S8) at low temperatures, which might stem from adsorbed CO from air as pointed out by Zhou et al.[28a] However, this peak cannot be assigned unambiguously. We found a low CO_2-desorption (Figure 5 (b), Figure S33–S35) at high temperatures (< 830 °C), which could be due to pyrone-type structures or reactions of desorbing CO with surface-bound O.[28c,29] The CO_2-desorption peak slightly below 200 °C (Pt/ROX, Pt/DARCO) might be assigned to adsorbed CO_2 on the surface of the catalysts. For Pt/CN1, we observed a CO-desorption peak at around 620 °C (Figure 5 a)) with a broad H_2O signal overlaying at around 630 °C (not shown). While we believe that these two signals have the same source, the delay can be caused by partial condensation of H_2O in the pipes to the MS. We assume that the peak at 620 °C is related to desorption of phenol groups, which dominated the surface with a share of > 50 % in the CO-signal. None of the other supports gave a significant H_2O-desorption signal in this range, meaning that there were none or minor phenol species present on the surface. This peak and the desorption of H_2O were even more pronounced in the raw support material (Figure 5 c) and Figure S43), supporting the assignment of phenol functions. Pt/ROX and Pt/DARCO also showed a broad CO-desorption peak at almost the same temperature but with lower intensity (fraction ≤ 15 %), meaning that there is another CO releasing group overlapping. Decomposition of ether functions, which were assigned to a close desorption temperature of about 700–750 °C, might overlap. As mentioned by Zhou et al., the location of functional groups at different positions in the carbon structure can lead to a variation in the decomposition temperature.[28a] Hence, the H_2O-desorption signal should be taken into account when assigning phenol/alcohol functions.

Fitting of the desorption-data was performed to estimate the fraction of different functional groups contributing to the chemical properties of the support materials. Due to the complex, heterogeneous nature of the materials a precise fitting of all species was not feasible and a simple fitting model was used. Detailed information about the general assignment of the functional groups can be found in the references in the experimental section. In contrast to the results of Wan et al. and Zhou et al., we observed the lowest FDCA yield for the Pt/CN1 catalyst. Pt/CN1 was particularly rich in phenol groups, which seem to have a negative influence on the catalytic activity.[5,13] Pt/ROX and Pt/DARCO, whose supports had a similar share of

graphite domains, gave significant differences in the CO- and CO_2-desorption profiles. In general, the CO_2-desorption signal was weaker compared to the CO signal, implying rather a correlation of the activity of the activated carbons with CO desorbing functions. Pt/ROX displayed two high temperature CO_2-desorption peaks centered at around 580 to 700 °C. These peaks were assigned to different lactone/ester species. Pt/ROX showed a considerable peak, which is visible as a shoulder in the overlaying signals, assigned to quinone or pyrone-type decomposition in the CO signal (Figure 5 (a)) at the highest assigned desorption temperature of about 875 °C. This peak could only be assigned for Pt/ROX, while the other catalysts gave no peak in this regime. Interestingly, this peak was present as a distinct peak in the raw support material, while the final catalyst showed an overlapping carbonyl signal. This might arise from a general higher intensity of ether functions (~750 °C in the CO-signal) of all catalysts compared to their bare supports, being more difficult to reduce or a product of the catalyst reduction.

Li et al. proposed that quinone functions could catalyze the alcohol oxidation including proton abstraction from hydroxyl and hydrogen abstraction from α-CH.[24] We assume that the higher reaction rate of Pt/ROX compared to the other activated carbon-based catalysts can be explained either by a redox mediator effect of quinone, as also suggested by Zhou et al., or the considerable basicity of pyrone-type functions, which might abstract protons and generate hydroxyl ions.[13,25,28a,c] Pyrone-type species contain non-neighboring ether and carbonyl functions, which were shown to contribute to the basicity of the support by resonance stabilization of the positive charge in a conjugated system.[25–26] Moreover, the high temperature CO_2-desorption peak for lactones in Pt/ROX might be related to pyrone-type functions with the ether being adjacent to the carbonyl function (lactone). In comparison to Pt/ROX, Pt/DARCO had the CO desorption peak with the highest fraction (58%) at a lower temperature, which is assigned to carbonyl functions, resulting in the lower catalytic activity.

When comparing the fresh catalysts with the raw supports, it is visible that all profiles, which were derived from the supports, showed a higher intensity and an improved signal-to-noise ratio. This might be caused by a general reduction of functional groups by hydrogen, reducing the concentration of O-containing functions on the surface of the reduced catalysts. Interestingly, the peak profiles of the supports showed a similar profile to the final catalysts with only minor shifts and changes in the intensity. Nevertheless, the specific features of the different support materials were preserved upon the reduction of $Pt(NO_3)_2$.

Probing of functional groups with XPS (Figure 6) is complementary to TPD, since mainly functions on the surface of the carbons are assessed. We applied three peaks, at 1.) 531.25 ± 0.25 eV assigned to carbonyl (ketone in conjugated π-system, quinone, lactone and carboxylic acid),[30] 2.) 532.3 ± 0.2 eV attributed to ether and carbonyl (lactone, anhydride, and aliphatic ketone),[30a,31] and 3.) 533.4 ± 0.2 eV assigned to phenolic, single bonded O in a conjugated π-system, and OH in carboxylic acid (Figure S44–S48 and Table S10).[30b,e, 32] The

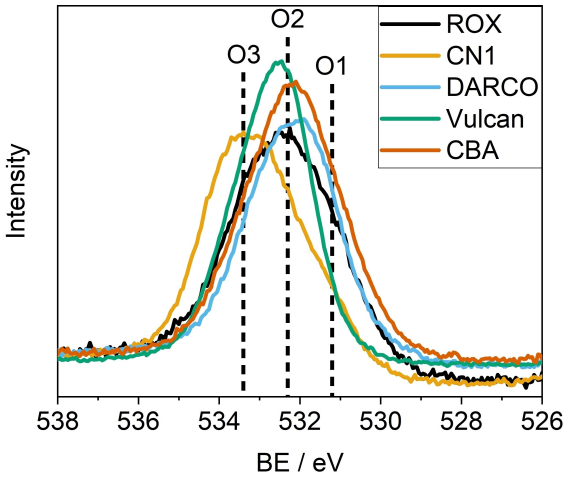

Figure 6. O1s XPS spectra of ROX, CN1, DARCO, Vulcan, and CBA.

species fitted around 532.5 eV are often referred to as aliphatic C–O. However, this assignment is not in agreement with our TPD fits, which display a high concentration of carbonyl containing species for samples with high share of the O2 component like DARCO.[33] Therefore, we conclude that this component includes carbonyl species.[30a] Carbonyls in carboxylic acids are sometimes also assigned to a peak around 532.5 eV.[24]

Due to an O-content < 0.1%, in particular the O1s peak for CBA might also be attributed to the presence of adventitious hydrocarbon adsorption.[34] In general, their presence can lead to uncertainties in the measurements, however, for samples with high O-content the influence is expected to be negligible. The XPS spectrum confirmed the TPD results for CN1, with a high concentration of single-bonded O with higher binding energy corresponding to phenolic functions on the surface.[30b,c,32] For ROX, the fit had an almost equal distribution of all three O species. The reason can be the high concentration of lactone and pyrone-type species, which add equally to O1 and O3 components. In addition, quinone might be allocated to O1 and carbonyl and ethers for the O2 components. Also Weippert et al. and Langley et al., assigned lactone species to O1 and O3, and quinone species to O1.[30c,d] For DARCO, we observed a narrower peak with a dominant O2 species. Hence, this peak is assigned to a carbonyl species desorbing at lower temperatures than quinone and pyrone-type, which is in agreement with TPD results, in addition to ether functions contributing to the O2 component. Both quinone and pyrone-type functions are related to extended conjugated systems for resonance stabilization. Therefore, DARCO provides a significantly lower concentration of redox active O-functions, which are important for the oxidation process. These functional groups are the reason for the higher activity of Pt/ROX compared to Pt/DARCO, although both supports have a similar O-content and a similar graphitization degree. Pyrone-type and quinone functions might take abstracted protons from the surface of the Pt particles and act as a co-catalyst during the

reactivation of the Pt particles and generation of OH^- ions from dissociated O_2.[35]

C 1 s spectra were also recorded. Note that fitting proved to not be practical owing to the heterogeneous nature of the support materials leading to a broad asymmetric peak without distinct features (Figure S49–S53). This might be caused by the presence of various slightly different species and environments of the C atoms, as pointed out by Gengenbach et al.[34] In addition to the correlation of the support properties and the catalytic activity, the influence on the stability of the supported Pt particles and possible deactivation mechanism of the catalysts were investigated. The anchoring of Pt particles via, e.g., carbonyl moieties, improved the stability against leaching.

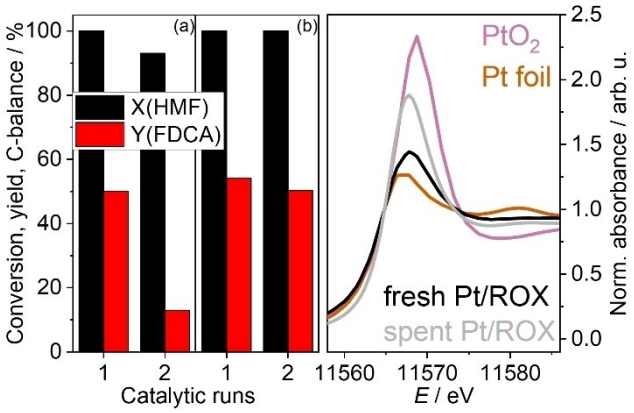

Figure 7. Left: Catalyst recycling with (a) direct reuse and (b) additional reduction with H_2 after the catalyst recovery. Right: XANES spectra of Pt/ROX catalyst before and after HMF oxidation (100 °C, 30 bar air, 5 h) measured at Pt L_3-edge. Pt foil and PtO_2 references are shown.

Recyclability and Stability

Interestingly, the nanoparticles showed differences in the stability depending on the support material, particularly due to leaching of Pt, in addition to the observed influence on the activity (cf. Figure S56). The anchoring of Pt particles via O-containing surface sites on the carbon support was crucial for the differences in the stability. It probably occurred during the reduction process by formation of Pt–O bonds with the support material during particle formation. The two carbon black supports Vulcan and CBA had the highest C-content and the lowest O-content as determined by elemental analysis. This caused a weaker interaction with the support and lead to the highest concentration of leached Pt into the solution. Particularly, Pt/CBA with an O-content $<0.1\,\%$ and a high graphitization degree showed leaching of Pt species to the solution. However, it could be shown by hot filtration tests that leached Pt species do not contribute considerably in a homogeneous manner to the observed catalytic activity (cf. Figure S55). Since we observed a linear increase of the FDCA yield for Pt/CBA over 7 h, these weakly bound Pt-species are not catalytically active. Surprisingly, the support with the highest O-content (CN1) did not show the best stability. Thus, the high concentration of OH groups might lead to a weaker interaction of Pt and the support, possibly due to its more acidic nature. Therefore, the overall O-content was not the decisive factor and specific functional groups lead to a better metal-support interaction. Pt/DARCO gave the best stability in terms of leaching (Figure S56) under reaction conditions (100 °C, 30 bar). The support showed a higher carbonyl concentration compared to e.g. ROX. It was shown in literature that leaching of noble metal species from carbon-based supports was particularly pronounced for Pt-based catalysts compared to Au, Pd or Ru.[4a]

To study the reusability of Pt/ROX, which showed less leaching, we separated the catalyst after the reaction by centrifugation and washed it with water. Thereby, we observed a drastic decrease of the FDCA yield in a second run (5 h; cf. Figure 7). In the ex-situ XANES analysis of the catalyst before and after the reaction (Figure 7), we saw a clear increase in the height of the white line feature at Pt L_3-edge, meaning that Pt got significantly oxidized during the reaction under base-free conditions. However, the spectrum still contains features of metallic Pt, indicating that only the surface of the Pt-particles was oxidized causing the loss of activity.

We performed an additional experiment with the catalyst being reduced after the first run in 10 % H_2/N_2 (3 L min^{-1} at 350 °C for 2 h). Interestingly, the catalyst maintained the activity for a second run. The small difference can be explained by the above mentioned leaching of Pt and some loss of catalyst powder during separation of the catalyst after the reaction. Furthermore, no appearance of Pt reflections in the XRD was observed after the reaction excluding sintering as cause of the deactivation (cf. Figure S57). Due to an approximately linear increase of the FDCA yield over 7 h reaction, we assume that Pt particles are only oxidized towards the end of the reaction, when alcohol and aldehyde functions of the reactants are mostly consumed. Thus, the results show that metallic Pt is the active phase, and emphasize the importance of reduction steps after each run to maintain the activity for the base-free oxidation of HMF in batch processes. A continuous flow process might help to overcome this issue, if continuously new reactant is fed as shown by Liguori et al., who observed no decrease in the activity over 44 h time-on-stream.[36]

In addition, we performed Raman spectroscopy of spent Pt/ROX and Pt/CBA catalysts (100 °C, 30 bar air, 7 h) to examine potential changes in the Carbon structure (Figure S58–S59). Only minor changes in the intensity of the peaks but no variations in the peak profile were observed.

Pt/ROX was also characterized by TPD after the oxidation of HMF (100 °C, 30 bar air, 7 h). The catalyst was separated from the reaction solution by centrifugation and washed two times with water. It has to be noted that the results are affected by the presence of adsorbed organic residues on the catalyst surface, which could not be removed completely by washing. These residues cause intense desorption peaks of H_2O, CO, and CO_2 in a range of 100 °C to about 450 °C (cf. Figure S60). The features in the signal of the CO_2 desorption (Figure S61 (a)) of the spent Pt/ROX catalyst showed mainly desorption of organic residues. In the CO desorption signal (Figure S61 (b)), a peak at about 780 °C was observed. This peak was also present in the

fresh Pt/ROX catalyst, however, it is shifted to a lower desorption temperature. The peak was assigned to pyrone-type or quinone species for the fresh catalyst, but the lower desorption temperature fits better to carbonyl species. The uptake of protons by cyclic pyrone-type functions might lead to the formation of an aliphatic aldehyde (see structure in Figure 8).[25] Aldehyde functions have a lower desorption temperature. The uptake of protons by quinone functions results in the formation of alcohol functions with an even lower desorption temperature at around 600 °C. Thus, the participation of pyrone-type functions in the reaction might have resulted in the transformation of the functional groups, which causes the need for a reactivation.

Conclusions

Pt-catalysts supported on activated carbon and carbon black have been found very attractive for the selective oxidation of HMF to FDCA, an important monomer for a future bio-based chemical industry. The advantage of this approach is that HMF can be transformed in complete absence of a homogeneous base, which avoids waste from neutralization for product separation, in addition to the use of air as a sustainable oxidant, and water as a green solvent. The chemical properties of some activated carbon and carbon black enabled the efficient substitution of the homogeneous base. The catalytic activity strongly depends on the kind of C-support, and their structural and chemical properties (graphite domains, O-functionalities). The role of activated carbon and carbon black was studied systematically by ensuring a similar Pt particle size and loading. Of all tested C-supported Pt-catalysts, Pt/CBA and Pt/ROX gave the highest FDCA yields of 87 % and 75 %, respectively, which ranks them as highly active compared to other catalysts reported in literature.

We observed that the support composition, in particular graphene domains for carbon black, and quinone and pyrone-type functional groups for activated carbons, had a significant influence on the catalytic activity (Figure 8). Graphene layers on the surface of carbon black are proposed to contribute with their extended conjugated π-system through the delocalization of electrons from the Pt particles to the superior activity. The activity differed significantly from carbon black without graphene layers. Quinone and pyrone-type functional groups activated the alcohol moiety in HMF and generate hydroxide ions on the surface through their redox activity. In contrast, an activated carbon rich in phenol groups was found to yield the lowest activity. The stability of the active species might be improved in the future by a change, e.g. to AuPd alloys. The comprehensive characterization of the support structure and properties enable the knowledge-based selection of catalysts for the selective, sustainable, base-free oxidation of HMF. Thus, the decisive role of activated carbon and carbon black found in this work may also further guide the production of other highly active Carbon-based catalysts.

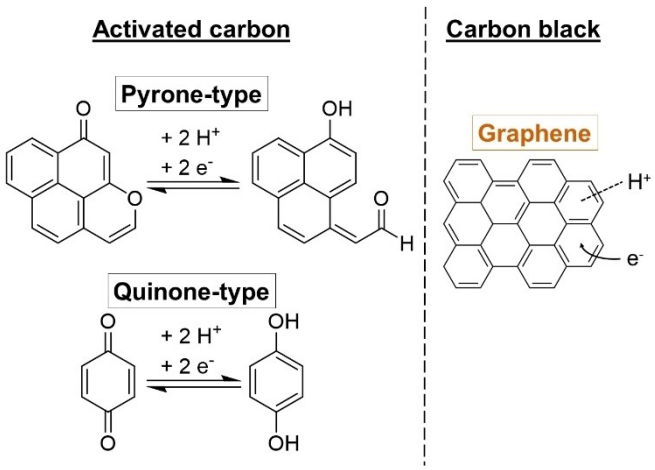

Figure 8. Rate-enhancing role of different carbon support properties (black: activated carbon ROX, dark orange: carbon black CBA).

Experimental Section

Catalyst Preparation

All catalysts were prepared by incipient-wetness impregnation. $Pt(NO_3)_2$ (0.0656 g) was dissolved in a volume of water equal to the pore volume of the support. The solution was added dropwise to NORIT® ROX (ROX), NORIT® CN1 (CN1), NORIT® DARCO (DARCO), VULCAN® XC-72 (Vulcan), or carbon black acetylene (CBA), respectively, (1.96 g) under careful stirring with a plastic spatula over a few minutes (further details on the support materials are given in Table S1, S6, and S7). For carbon black supports, a 1 : 1 ethanol/water mixture was used. Afterwards, the catalysts were dried at 80 °C overnight, followed by reduction at 350 °C for 2 h (heating: 5 °C/min) in a flow of 10 % H_2 in N_2 (3 l/min).

Catalyst and Support Characterization

Electron microscopy images of the catalysts were taken by scanning transmission electron microscopy (STEM; ThermoFisher Themis 300 (S)TEM). A high-angle annular dark-field (HAADF) detector was used for improving the contrast between heavier and lighter elements. Energy dispersive X-ray (EDX) mapping was recorded with a ThermoFisher Scientific Super-X EDX detector. The catalysts were prepared on a standard Lacey carbon grid with Cu mesh. Agglomerated particles were not considered in the particle size distribution.

X-ray absorption spectroscopy (XAS) measurements of the catalysts and the reference samples were performed at the BM23 beamline[37] at ESRF (European Synchrotron Radiation Facility) and the P65 beamline[38] at PETRA III (Deutsches Elektronen Synchrotron), using the Pt L_3-edge (11.564 keV). Samples were measured as powder in polypropylene tubes with 6 mm diameter in transmission mode. The intensity was recorded with ionization chambers. Data treatment and analysis was performed using Athena from the Demeter software package (version 0.9.26).[39]

X-ray photoelectron spectroscopy (XPS; SPECS Phoibos 150 analyser) of the supports was conducted applying a non-monochromatic XR-50 Mg K_α X-ray source and an angle of 45 ° between analyzer and X-ray source. The energy scale was calibrated by a Ag reference. Charging effects were minimized with a flood gun. Data processing was performed with the CasaXPS software using graph-

itic carbon for energy calibration and subtracting a Shirley background.[40] A 50:50 Gaussian and Lorentzian peak shape was chosen for fitting the O1s peaks. The same FWHM (1.5–2.3) was used for all peaks in each spectrum. Due to the heterogeneous nature of the materials, it was not possible to distinguish more species.

TPD (Netzsch STA 449 F3 Jupiter) of the supports was conducted using 30–50 mg of sample mass. The sample was flushed with 80 mL min^{-1} of Ar for about 16 h before heating the sample in the same flow to 1200 °C with 5 °C min^{-1}. The gas composition at the outlet was monitored by mass spectrometry (MS; Netzsch QMS 403 D Aëolos). The data for the CO and CO_2 profiles were fitted with Origin2019 using Gauss functions.

Raman spectra (Renishaw inVia Raman spectrometer) of the supports were recorded using a frequency doubled Nd:YAG laser (532 nm, ~100 mW at the source) and an optical microscope (Leica). The support powders were pressed to obtain a flat surface before measurement. Five spectra were measured at different spots in a range from 500 to 4000 cm^{-1}. The spectra were averaged and baseline-corrected. To estimate the share of sp^2-hybridized C in graphite or graphene structures, we fitted Lorentz functions to the Raman spectra with Origin 2019. Five peaks (D1 ≈ 1345 cm^{-1}, D2 ≈ 1620 cm^{-1}, D3 ≈ 1500 cm^{-1}, D4 ≈ 1185 cm^{-1} and G ≈ 1590 cm^{-1}) were taken into account. The same restrictions for FWHM and peak positions were used for the fitting of all spectra.

Additional experimental information and data can be found in the supporting information. Raw data are available from https://doi.org/10.35097/1881.

Acknowledgements

The authors would like to thank Alexandra Böhm (elemental analysis), Maria Casapu (assistance in TPD), Veronika Holderied (assistance with HPLC), Armin Lautenbach (ICP-OES), Marion Lenzner (TG analysis), Markus Makowiak (nitrogen physisorption), Shweta Sharma (assistance in STEM), and Matthias Stehle, Linda Klag and Andrea De Giacinto (assistance in Raman spectroscopy). We acknowledge DESY (Hamburg, Germany), a member of the Helmholtz Association HGF, and ESRF (Grenoble, France) for the provision of synchrotron light. The measurements were performed in the frame of the proposals CH 6119 (ESRF) and I-20211473 (DESY) at BM23 and P65 beamline, respectively. We would like to thank Edmund Welter and Cesare Atzori for assistance. We thank Bidyut B. Sarma for help in conducting the XAS experiments and data analysis. STEM imaging was carried out with the support of the Karlsruhe Nano Micro Facility (KNMFi, www.knmf.kit.edu), a Helmholtz Research Infrastructure at Karlsruhe Institute of Technology (KIT). We acknowledge the German Research Foundation DFG (INST 121384/73-1) for funding a Raman spectrometer. This work was financially supported by the Federal Ministry of Food and Agriculture (BMEL) through the FNR (Fachagentur Nachwachsende Rohstoffe e. V.) based on a decision taken by the German Bundestag (funding no. 22010718). Open Access funding enabled and organized by Projekt DEAL.

Conflict of Interests

The authors declare no conflict of interest.

Data Availability Statement

The data that support the findings of this study are available from the corresponding author upon reasonable request. The raw data are available from https://doi.org/10.35097/1881.

Keywords: Carbon · Heterogeneous catalysis · HMF · Oxidation · Platinum · Sustainable chemistry

[1] a) R. A. Sheldon, *ACS Sustainable Chem. Eng.* **2018**, *6*, 4464–4480; b) M. Sajid, X. Zhao, D. Liu, *Green Chem.* **2018**, *20*, 5427–5453; c) J. J. Bozell, G. R. Petersen, *Green Chem.* **2010**, *12*, 539–554.
[2] a) K. Hengst, M. Schubert, W. Kleist, J.-D. Grunwaldt, in *Catalytic Hydrogenation for Biomass Valorization*, **2014**, pp. 125–150; b) P. N. R. Vennestrøm, C. M. Osmundsen, C. H. Christensen, E. Taarning, *Angew. Chem. Int. Ed.* **2011**, *50*, 10502–10509; c) C. H. Christensen, J. Rass-Hansen, C. C. Marsden, E. Taarning, K. Egeblad, *ChemSusChem* **2008**, *1*, 283–289.
[3] a) O. R. Schade, K. F. Kalz, D. Neukum, W. Kleist, J.-D. Grunwaldt, *Green Chem.* **2018**, *20*, 3530–3541; b) R.-J. van Putten, J. C. van der Waal, E. de Jong, C. B. Rasrendra, H. J. Heeres, J. G. de Vries, *Chem. Rev.* **2013**, *113*, 1499–1597.
[4] a) D. Neukum, L. Baumgarten, D. Wüst, B. B. Sarma, E. Saraçi, A. Kruse, J.-D. Grunwaldt, *ChemSusChem* **2022**, *15*, e202200418; b) S. Dutta, S. De, M. I. Alam, M. M. Abu-Omar, B. Saha, *J. Catal.* **2012**, *288*, 8–15.
[5] X. Wan, C. Zhou, J. Chen, W. Deng, Q. Zhang, Y. Yang, Y. Wang, *ACS Catal.* **2014**, *4*, 2175–2185.
[6] S. E. Davis, A. D. Benavidez, R. W. Gosselink, J. H. Bitter, K. P. de Jong, A. K. Datye, R. J. Davis, *J. Mol. Catal. A* **2014**, *388–389*, 123–132.
[7] D. Bonincontro, A. Lolli, A. Villa, L. Prati, N. Dimitratos, G. M. Veith, L. E. Chinchilla, G. A. Botton, F. Cavani, S. Albonetti, *Green Chem.* **2019**, *21*, 4090–4099.
[8] N. M. Julkapli, S. Bagheri, *Int. J. Hydrogen Energy* **2015**, *40*, 948–979.
[9] J. Artz, R. Palkovits, *ChemSusChem* **2015**, *8*, 3832–3838.
[10] H. Ait Rass, N. Essayem, M. Besson, *Green Chem.* **2013**, *15*, 2240–2251.
[11] H. Yu, K.-A. Kim, M. J. Kang, S. Y. Hwang, H. G. Cha, *ACS Sustainable Chem. Eng.* **2019**, *7*, 3742–3748.
[12] X. Han, C. Li, Y. Guo, X. Liu, Y. Zhang, Y. Wang, *Appl. Catal. A* **2016**, *526*, 1–8.
[13] C. Zhou, W. Deng, X. Wan, Q. Zhang, Y. Yang, Y. Wang, *ChemCatChem* **2015**, *7*, 2853–2863.
[14] W. Gu, G. Yushin, *Wiley Interdiscip. Rev.: Energy Environ.* **2014**, *3*, 424–473.
[15] A. Villa, M. Schiavoni, S. Campisi, G. M. Veith, L. Prati, *ChemSusChem* **2013**, *6*, 609–612.
[16] N. Sasirekha, P. Sangeetha, Y.-W. Chen, *J. Phys. Chem. C* **2014**, *118*, 15226–15233.
[17] a) Y. Y. Gorbanev, S. Kegnæs, A. Riisager, *Top. Catal.* **2011**, *54*, 1318; b) Y. Y. Gorbanev, S. Kegnæs, A. Riisager, *Catal. Lett.* **2011**, *141*, 1752–1760.
[18] a) C. Megías-Sayago, A. Lolli, D. Bonincontro, A. Penkova, S. Albonetti, F. Cavani, J. A. Odriozola, S. Ivanova, *ChemCatChem* **2020**, *12*, 1177–1183; b) O. Schade, P. Dolcet, A. Nefedov, X. Huang, E. Saraçi, C. Wöll, J.-D. Grunwaldt, *Catalysts* **2020**, *10*, 342.
[19] A. V. Kirilin, B. Hasse, A. V. Tokarev, L. M. Kustov, G. N. Baeva, G. O. Bragina, A. Y. Stakheev, A.-R. Rautio, T. Salmi, B. J. M. Etzold, J.-P. Mikkola, D. Y. Murzin, *Catal. Sci. Technol.* **2014**, *4*, 387–401.
[20] I. L. Simakova, Y. S. Demidova, J. Gläsel, E. V. Murzina, T. Schubert, I. P. Prosvirin, B. J. M. Etzold, D. Y. Murzin, *Catal. Sci. Technol.* **2016**, *6*, 8490–8504.
[21] B. Hasse, J. Gläsel, A. M. Kern, D. Y. Murzin, B. J. M. Etzold, *Catal. Today* **2015**, *249*, 30–37.
[22] A. Sadezky, H. Muckenhuber, H. Grothe, R. Niessner, U. Pöschl, *Carbon* **2005**, *43*, 1731–1742.
[23] Z. Ni, Y. Wang, T. Yu, Z. Shen, *Nano Res.* **2008**, *1*, 273–291.

[24] F. Li, P. Yan, F. Herold, A. Drochner, H. Wang, T. Cao, W. Liu, X. Dai, B. Zhang, B. J. M. Etzold, W. Qi, *Carbon* **2020**, *170*, 580–588.
[25] M. A. Montes-Morán, D. Suárez, J. A. Menéndez, E. Fuente, *Carbon* **2004**, *42*, 1219–1225.
[26] C. A. Leon y Leon, J. M. Solar, V. Calemma, L. R. Radovic, *Carbon* **1992**, *30*, 797–811.
[27] A. Cuesta, P. Dhamelincourt, J. Laureyns, A. Martínez-Alonso, J. M. D. Tascón, *J. Mater. Chem.* **1998**, *8*, 2875–2879.
[28] a) J.-H. Zhou, Z.-J. Sui, J. Zhu, P. Li, D. Chen, Y.-C. Dai, W.-K. Yuan, *Carbon* **2007**, *45*, 785–796; b) M. Thommes, C. Morlay, R. Ahmad, J. P. Joly, *Adsorption* **2011**, *17*, 653–661; c) G. S. Szymański, Z. Karpiński, S. Biniak, A. Świa˛tkowski, *Carbon* **2002**, *40*, 2627–2639; d) J. L. Figueiredo, M. F. R. Pereira, M. M. A. Freitas, J. J. M. Órfão, *Carbon* **1999**, *37*, 1379–1389; e) G. de la Puente, J. J. Pis, J. A. Menéndez, P. Grange, *J. Anal. Appl. Pyrolysis* **1997**, *43*, 125–138.
[29] H. P. Boehm, *Carbon* **2002**, *40*, 145–149.
[30] a) U. Zielke, K. J. Hüttinger, W. P. Hoffman, *Carbon* **1996**, *34*, 983–998; b) D. Rosenthal, M. Ruta, R. Schlögl, L. Kiwi-Minsker, *Carbon* **2010**, *48*, 1835–1843; c) L. A. Langley, D. E. Villanueva, D. H. Fairbrother, *Chem. Mater.* **2006**, *18*, 169–178; d) J. Weippert, V. Gewiese, A. Böttcher, M. M. Kappes, *J. Phys. Chem. C* **2018**, *122*, 28601–28612; e) A. Ganguly, S. Sharma, P. Papakonstantinou, J. Hamilton, *J. Phys. Chem. C* **2011**, *115*, 17009–17019.
[31] C. Hontoria-Lucas, A. J. López-Peinado, J. d. D. López-González, M. L. Rojas-Cervantes, R. M. Martín-Aranda, *Carbon* **1995**, *33*, 1585–1592.
[32] A. P. Terzyk, *Colloids Surf. A: Physicochem. Eng. Asp.* **2001**, *177*, 23–45.
[33] M. Smith, L. Scudiero, J. Espinal, J.-S. McEwen, M. Garcia-Perez, *Carbon* **2016**, *110*, 155–171.
[34] T. R. Gengenbach, G. H. Major, M. R. Linford, C. D. Easton, *J. Vac. Sci. Technol. A* **2021**, *39*, 013204.
[35] S. E. Davis, B. N. Zope, R. J. Davis, *Green Chem.* **2012**, *14*, 143–147.
[36] F. Liguori, P. Barbaro, N. Calisi, *ChemSusChem* **2019**, *12*, 2558–2563.
[37] O. Mathon, A. Beteva, J. Borrel, D. Bugnazet, S. Gatla, R. Hino, I. Kantor, T. Mairs, M. Munoz, S. Pasternak, F. Perrin, S. Pascarelli, *J. Synchrotron Radiat.* **2015**, *22*, 1548–1554.
[38] E. Welter, R. Chernikov, M. Herrmann, R. Nemausat, *AIP Conf. Proc.* **2019**, *2054*, 040002.
[39] B. Ravel, M. Newville, *J. Synchrotron Radiat.* **2005**, *12*, 537–541.
[40] N. Fairley, A. Carrick, N. Fairly, *The casa cookbook, Vol. 1*, Acolyte science Cheshire, **2005**.

Manuscript received: November 27, 2023
Revised manuscript received: February 6, 2024
Accepted manuscript online: February 7, 2024
Version of record online: March 8, 2024